

Photovoltaic properties of $\text{Bi}_2\text{FeCrO}_6$ epitaxial thin films

R. Nechache,^{1,2} C. Harnagea,² S. Licoccia,¹ E. Traversa,^{1,3} A. Ruediger,¹ A. Pignolet,² and F. Rosei^{2,4,a)}

¹Department of Chemical Science and Technology and NAST Center, University of Rome, Tor Vergata Via della Ricerca Scientifica 1, 00133 Rome, Italy

²Centre Énergie, Matériaux et Télécommunications, INRS, 1650, boulevard Lionel-Boulet, Varennes, Québec J3X 1S2, Canada

³International Research Center for Materials Nanoarchitectonics (MANA), National Institute for Materials Science (NIMS), Namiki, Tsukuba, Ibaraki 305-0044, Japan

⁴Center for Self-Assembled Chemical Structures, McGill University, Montreal, Quebec H3A 2K6, Canada

(Received 2 March 2011; accepted 20 April 2011; published online 19 May 2011)

We report a large photovoltaic (PV) effect in multiferroic $\text{Bi}_2\text{FeCrO}_6$ (BFCO) films under monochromatic illumination at 635 nm with an intensity of 1.5 mW cm^{-2} . These multiferroic films exhibit a large photocurrent at zero bias voltage and an open-circuit voltage of about 0.6 V. A high PV power conversion efficiency of about 6% for red light is achieved and attributed to a high degree of B-site cationic ordering between Fe and Cr sublattices, the tuning of which is likely to play a key role in further improvements of the PV properties in BFCO. © 2011 American Institute of Physics. [doi:10.1063/1.3590270]

The bulk photovoltaic (PV) effect observed in ferroelectric perovskite thin films (Refs. 1 and 2) has regained attention due to its potential for optoelectronics, energy conversion, and optical information storage.^{3,4} Anomalous bulk PV (BPV) currents were originally observed in ferroelectric oxides, e.g., LiNbO_3 and $\text{Pb}(\text{Zr},\text{Ti})\text{O}_3$ (PZT).⁵⁻⁷ In contrast to the conventional junction-based interfacial PV effect in semiconductors, with the BPV effect in ferroelectrics the photo-generated charge carriers of both polarity are driven toward cathode/anode, by the polarization-induced internal electric field that extends over the whole volume. Therefore, in contrast to the junction case, where the field is only present in a thin depletion layer at the interface, charge transport through ferroelectrics is not primarily limited by diffusion and no low-energy barrier affects the output photovoltage.⁸ The obtained BPV efficiencies however are low, typically 10^{-7} – 10^{-5} , mainly due to the large band gap in most bulk ferroelectrics (3–4 eV) and the resulting low cross-sections for photoexcitation in the visible range.^{9,10}

In the case of ferroelectric thin films, other electric fields in addition to the BPV effect can contribute to photocurrents (e.g., space-charge fields induced by defects formed during fabrication),¹¹⁻¹⁴ giving rise to a complex interplay of phenomena that is still under investigation. The largest PV power conversion efficiency for ferroelectric films ($\sim 0.28\%$) recently achieved with devices based on epitaxial La-doped PZT films (Ref. 13) is limited by its large band gap (3.2–3.6 eV). Multiferroics possess a magnetic order parameter besides the ferroelectric one and the electron–electron interaction governing the magnetic ordering leads to a smaller gap [e.g., 2.6–2.7 eV for BiFeO_3 , (BFO)] (Refs. 15 and 16) than for the other ferroelectric perovskites. Thus, multiferroic oxides such as BFO and $\text{Bi}_2\text{FeCrO}_6$ (BFCO) (Refs. 17 and 18) should lead to higher PV efficiencies.

BFCO films have a remnant polarization of about $55 \mu\text{C}/\text{cm}^2$ along the [001] pseudocubic direction,¹⁹ and are

ferrimagnetic with a magnetic moment depending on Fe/Cr ordering,^{20,21} about $1.8 \mu_B$ per formula unit. The investigation of the optical properties in BFCO is in its infancy, and some theoretical studies predict a band gap range of 1.4–2.0 eV (Ref. 22) for ferrimagnetic-ferroelectric BFCO, corresponding to photosensitivity in the near infrared range.

In this letter, we describe the PV properties of BFCO thin film devices with indium tin oxide (ITO) top electrodes, reporting a high power conversion efficiency.

Two BFCO films were directly grown on (100)-oriented niobium doped- SrTiO_3 (STO:Nb) substrates²⁰ by pulsed laser deposition (PLD). The deposition temperature and oxygen partial pressure were $660 \text{ }^\circ\text{C}$ and 1×10^{-2} mbar for film A and $610 \text{ }^\circ\text{C}$ and 9×10^{-3} mbar for film B. The deposition rate was 0.15 nm/s and the films were grown for 14 min, resulting in a film thickness of 125 nm measured by Dektak profilometer. For these deposition parameters the BFCO films are epitaxial and single phase,¹⁹ as confirmed by x-ray diffraction (XRD) (Fig. 1). In both cases, the θ – 2θ XRD plots showed only the $00l$ ($l=1, 2, 3$) pseudocubic peaks from the BFCO films and STO:Nb substrates [Fig. 1(a)]. The calculated out-of-plane c lattice parameters based on the pseudocubic structure are 3.962 and 3.969 Å for films A and B, respectively.

The in-plane pseudocubic parameters were estimated to be 3.906 Å, close to that of the STO:Nb substrate. Thus the BFCO thin films crystallized in a distorted monoclinic structure with a large c/a ratio due to the in-plane compressive (compared to the bulk BFCO lattice parameter of 3.93 Å) strain caused by the lattice mismatch (0.64%) between film and substrate. The (111) asymmetric XRD pattern [Fig. 1(b)] for the films revealed a twofold superstructure in the $\langle 111 \rangle$ direction, while the pattern along the $\langle 110 \rangle$ direction did not exhibit any superstructure.^{19,23} Higher superstructure intensity was observed for film A, indicating a higher degree of ordering.

To investigate the films' PV properties, top ITO contacts (area of 0.1 mm^2) were deposited by PLD through shadow masks.²⁴ A red laser (635 nm, $1.5 \text{ mW}/\text{cm}^2$, normal inci-

^{a)}Author to whom correspondence should be addressed. Electronic mail: rosei@emt.inrs.ca.

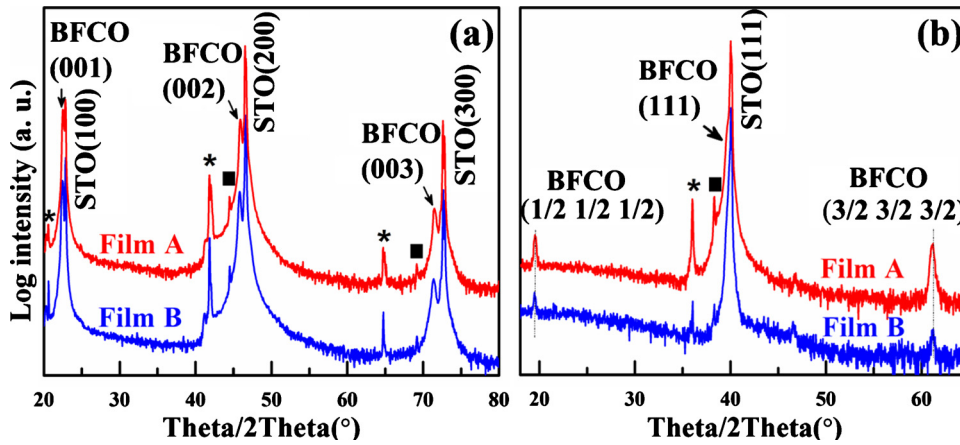


FIG. 1. (Color online) (001)-oriented BFCO structural characterization. (a) θ - 2θ and (b) (111) asymmetrical XRD scans for BFCO film A and B. The stars correspond to (00 l) K_{β} lines while the squares indicate tungsten contamination of the x-ray tube cathode.

dence) was used for the J - V measurements, performed with a HP4145A semiconductor parameter analyzer (Fig. 2, top-left inset).²⁵

In the J - V measurement, a positive bias voltage creates an electric field oriented bottom-to-top. The dark and illuminated J - V curves of the two epitaxial BFCO thin films are presented in Fig. 2. A diodelike behavior characterized by a directional leakage at positive voltage is observed for both films (Fig. 2). The J - V curves reveal a clear PV effect in both films. The open circuit photovoltage V_{oc} is about 0.74 V and 0.55 V for film A and B, respectively.

The highest short circuit photocurrent J_{ph} of about 0.99 mA/cm² is observed for film A (0.11 mA/cm² for film B). Both films exhibit a similar dark current, i.e., 3.7×10^{-3} mA/cm², which is negligible compared to the observed illuminated photocurrents. The power conversion efficiency η was calculated as $\eta = P_{out}^{max}/P_{in}$, where the input power density P_{in} (mW/cm²) is the radiation intensity received over the electrode surface, and $P_{out}^{max} = J_{ph}^{max} \times V_{oc}^{max}$ is the maximum output electrical power (Fig. 2, bottom-right inset). P_{out}^{max} for the films A and B are 0.097 and 0.012 mW/cm² respectively. A significantly higher external power efficiency η of 6.5% at a fill factor (FF) of about 0.13 [$FF = P_{out}^{max}/(V_{oc} \times J_{ph})$] was observed for film A.²⁶ The maximum external power conversion efficiency for film B was estimated to be 0.8% at $FF = 0.20$. Both films exhibit efficiencies that significantly exceed the theoretically pre-

dicted limit (10^{-6} – 10^{-7}) of the power conversion efficiency in ferroelectrics.²⁷ To ensure that the BPV and not interfacial effects are responsible for the observed behavior, we switched the direction of polarization in film A with an electric pulse. Consequently, both J_{ph} and V_{oc} were reversed (Fig. 2), their values being 0.38 mA/cm² and 0.41 V, respectively, below the values of the as-deposited film.

Fe–Cr ordering in BFCO causes a hybridization of the transition metals Fe and Cr d-bands with O 2 p . This large p - d hybridization (affected and possibly enhanced by the presence of the in-plane compressive strain) determines interatomic distances that lead to an optical band gap that efficiently absorbs red light. For a given band gap (related to the degree of Fe–Cr ordering, in turn controlled by the deposition conditions), photoconduction is determined by the charge carrier mobility in the conduction band, mainly composed of Fe 3 d and Cr 3 d states.^{28–30}

To elucidate the origin of the enhanced PV effect in the as-deposited samples, we studied the ferroelectric properties of the in-plane compressively strained epitaxial BFCO films using piezoresponse force microscopy (PFM),³¹ Fig. 3.³² Although in Figs. 3(a) and 3(d) an imprint is seen clearly only for A, both films exhibit it in the as-grown state being self-poled in a preferential direction. The PFM signal representing the polarization imprint is about three times higher for A than for B, indicating that the force driving the self-poling

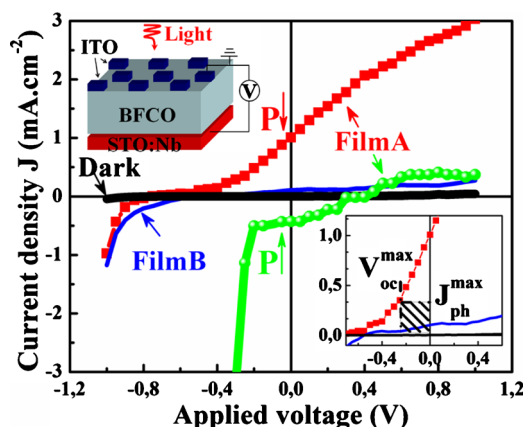


FIG. 2. (Color online) Dark and red light illumination J - V measurements curves revealing a PV effect in the BFCO epitaxial films. The top-left inset shows a schematic of the device. The bottom-right inset is a zoom around zero indicating for film A the maximum current density and open circuit voltage used for the calculation of the efficiency.

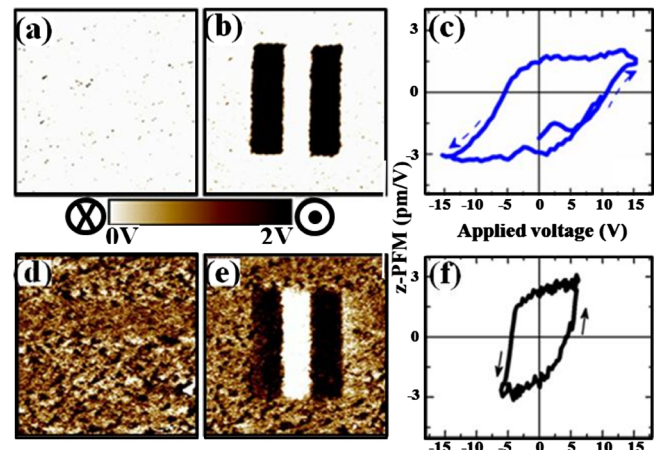


FIG. 3. (Color online) $10 \mu\text{m} \times 10 \mu\text{m}$ AFM image of (001)-oriented BFCO thin films deposited on STO:Nb (100) substrates. Out-of-plane PFM images: (a) as-grown and (b) after switching ferroelectric domains for film B; [(d) and (e)] for film A. [(c) and (f)] Ferroelectric hysteresis loops for film B and A, respectively.

process is much stronger for the film grown at higher temperature. To test for ferroelectricity, the polarization in both films was switched during scanning, by applying either negative or positive voltages between the conducting tip and the STO:Nb substrates [Figs. 3(b) and 3(e)]. Further analysis of the ferroelectric character of the BFCO films was performed by local remanent piezoelectric hysteresis loops as described elsewhere,³³ and confirmed polarization switching [Figs. 3(c) and 3(f)], also showing that the loop asymmetry decreases after several cycles, indicating a less pronounced imprint effect after cycling.³⁴

The prominent imprint in film A, with the ferroelectric polarization at zero external voltage preferentially directed toward the bottom electrode, ensures the presence of a strong internal electric field, driving the charges generated via photoelectric effect toward the electrodes, resulting in a large photocurrent.³⁵ When the ferroelectric is sandwiched between electrodes, the metal/ferroelectric interfaces can also participate to the photocurrent measured if they generate a conventional junction-based photocurrent.³⁶ The internal electric field in the ferroelectric is superimposed to the fields produced at the interfaces. To estimate the contribution of the BPV effect in our PV measurement we use the values for the J_{ph} and V_{oc} for the two opposite polarization directions and we find that the ferroelectric polarization generated internal electric field is the major contribution ($\sim 70\%$) to the observed PV effect.³⁶

In summary, we demonstrated a pronounced BPV effect at a wavelength of 635 nm in PLD-grown epitaxial multiferroic BFCO thin films compressively strained in-plane. Unprecedented high power conversion efficiency for ferroelectrics was demonstrated in 125 nm-thick highly ordered BFCO films. The results indicate that the ferroelectric polarization plays a dominant role in the observed PV effect. Further investigations are under way to measure the overall quantum conversion efficiency and mobility, and to determine in detail the effect of cation ordering on the PV properties of BFCO epitaxial films as well as BFCO submicron and nanostructures.³⁷

We acknowledge infrastructure support from the Canada Foundation for Innovation. F.R. is grateful to the Canada Research Chairs Program for partial salary support. A.P., A.R., and F.R. are supported by discovery grants (NSERC). F.R. thanks MDEIE (Quebec) for an international collaboration grant. S.L. and F.R. are supported by the Italian Ministry of Foreign Affairs (M.A.E.). We thank L.-P. Carignan and D. Menard (École Polytechnique Montreal) for technical support in the magnetic measurements. R.N. thanks JSPS for supporting his visit to MANA-NIMS (Tsukuba).

¹Y. S. Yang, S. J. Lee, S. Yi, B. G. Chae, S. H. Lee, H. J. Joo, and M. S. Jang, *Appl. Phys. Lett.* **76**, 774 (2000).

²P. S. Brody and B. J. Rod, *Integr. Ferroelectr.* **3**, 245 (1993).

³J. F. Scott and C. A. Araujo, *Science* **246**, 1400 (1989).

⁴H. Lin, N. J. Wu, F. Geiger, K. Xie, and A. Ignatiev, *Appl. Phys. Lett.* **66**, 1172 (1995).

⁵A. M. Glass, D. von der Linde, and T. J. Negran, *Appl. Phys. Lett.* **25**, 233 (1974).

⁶A. M. Glass, D. von der Linde, D. H. Auston, and T. J. Negran, *J. Electron. Mater.* **4**, 915 (1975).

⁷P. S. Brody and F. Crowne, *J. Electron. Mater.* **4**, 955 (1975).

⁸K. Yao, B. K. Gan, M. Chen, and S. Shannigrahi, *Appl. Phys. Lett.* **87**, 212906 (2005).

⁹V. M. Fridkin, *Crystallogr. Rep.* **46**, 654 (2001).

¹⁰The relatively short lifetime of the photo-induced charge carriers contributes to the low current densities (of the order of nA/cm²). From the engineering point of view, the internal resistance of these current sources is too large for their use as a power source.

¹¹V. S. Dharmadhikari and W. W. Grannemann, *J. Appl. Phys.* **53**, 8988 (1982).

¹²L. Pintilie, M. Alexe, A. Pignolet, and D. Hesse, *Appl. Phys. Lett.* **73**, 342 (1998).

¹³M. Qin, K. Yao, and Y. C. Liang, *Appl. Phys. Lett.* **93**, 122904 (2008).

¹⁴A. Kholkin, O. Boiarkine, and N. Setter, *Appl. Phys. Lett.* **72**, 130 (1998).

¹⁵S. R. Basu, L. W. Martin, Y.-H. Chu, M. Gajek, R. Ramesh, R. C. Rai, X. Xu, and J. L. Musfeldt, *Appl. Phys. Lett.* **92**, 091905 (2008).

¹⁶A. J. Hauser, J. Zhang, L. Mier, R. A. Ricciardo, P. M. Woodward, T. L. Gustafson, L. J. Brillson, and F. Y. Yang, *Appl. Phys. Lett.* **92**, 222901 (2008).

¹⁷R. Nechache, C. Harnagea, A. Pignolet, F. Normandin, T. Veres, L.-P. Carignan, and D. Ménard, *Appl. Phys. Lett.* **89**, 102902 (2006).

¹⁸R. Nechache, C. Harnagea, A. Pignolet, L.-P. Carignan, and D. Ménard, *Philos. Mag. Lett.* **87**, 231 (2007).

¹⁹R. Nechache, C. Harnagea, L.-P. Carignan, O. Gautreau, L. Pintilie, M. P. Singh, D. Menard, P. Fournier, M. Alexe, and A. Pignolet, *J. Appl. Phys.* **105**, 061621 (2009).

²⁰R. Nechache, L. Gunawan, L.-P. Carignan, C. Harnagea, G. Botton, D. Ménard, and A. Pignolet, *J. Mater. Res.* **22**, 2102 (2007).

²¹N. Ichikawa, M. Arai, Y. Imai, K. Hagiwara, H. Sakama, M. Azuma, Y. Shimakawa, M. Takano, Y. Kotaka, M. Yonetani, H. Fujisawa, M. Shimizu, K. Ishikawa, and Y. Cho, *Appl. Phys. Express* **1**, 101302 (2008).

²²Q.-X. Zhao, M.-X. Wen, S.-B. Wang, L. Guan, and B.-T. Liu, *J. Synth. Cryst.* **37**, 1390 (2008) (in Chinese).

²³Such superstructure originates from the rock-salt type ordering of B site cations in the BFCO double perovskite unit cell. As expected from the chosen deposition parameters, more detailed analyses indicate that the main difference between the two films is the intensity of the superlattice peaks, which is correlated with the degree of Fe/Cr cation ordering.

²⁴The shadow masks consist in a hexagonal arrays of circular holes 0.4 mm diameter with a periodicity of 1.2 mm.

²⁵The as-deposited samples were not electrically poled before measurements.

²⁶The FF is graphically measured as the area of the largest rectangle which will fit in the J - V curve.

²⁷V. M. Fridkin, *Crystallogr. Rep.* **46**, 654 (2001).

²⁸P. Baettig and N. A. Spaldin, *Appl. Phys. Lett.* **86**, 012505 (2005).

²⁹The repulsion mechanism could be at the origin of the decrease in power conversion efficiency observed in the less ordered film B.

³⁰Further investigation is in progress to analyze the optical and electrical properties of BFCO epitaxial thin films in relation with cation ordering.

³¹R. Nechache, C. Harnagea, A. Ruediger, F. Rosei, and A. Pignolet, *Func. Mater. Lett.* **3**, 83 (2010).

³²This technique probes the ferroelectric or piezoelectric nature of polar films and nanostructures with a resolution in the tens of nm range.

³³C. Harnagea, A. Pignolet, M. Alexe, D. Hesse, and U. Goesele, *Appl. Phys. A: Mater. Sci. Process.* **71**, 261 (2000).

³⁴This also indicates an initial difference in magnitude of the as-grown polarization, about three times higher for sample A.

³⁵This polarization imprint-induced internal electric field most likely originates from electrode-film interface effects (nonohmic contact, polarization pinned by defects).

³⁶F. Zheng, J. Xu, L. Fang, M. Shen, and X. Wu, *Appl. Phys. Lett.* **93**, 172101 (2008).

³⁷R. Nechache, C. V. Cojocar, C. Harnagea, C. Nauenheim, M. Nicklaus A. Ruediger, F. Rosei, and A. Pignolet, *Adv. Mater. (Weinheim, Ger.)* **23**, 1724 (2011).